Ge *et al. Satellite Navigation* (2023) 4:8
https://doi.org/10.1186/s43020-023-00097-3

Satellite Navigation
https://satellite-navigation.springeropen.com/

ORIGINAL ARTICLE Open Access

A new receiver clock model to enhance BDS-3 real-time PPP time transfer with the PPP-B2b service

Yulong Ge[1,7], Qing Wang[2*], Yong Wang[3,8], Daqian Lyu[4], Xinyun Cao[5], Fei Shen[5] and Xiaolin Meng[6]

Abstract

A new Precise Point Positioning (PPP) service, called the PPP-B2b service, has been implemented in the BeiDou-3 Navigation Satellite System (BDS-3), which brings new opportunities for time transfer. However, the solution using the traditional PPP method with the PPP-B2b correction still absorbs some unknown errors and needs reconverging when there exist abnormal data. We developed a new receiver clock model to improve PPP time transfer using the PPP-B2b correction. The traditional PPP time transfers using PPP-B2b with BDS-3, Global Positioning System (GPS), and BDS-3/GPS (Scheme1) are compared with the corresponding time transfer with the proposed clock model (Scheme2). The results show that GPS-only PPP is not recommended because of low accuracy of 2 ns. BDS-3 or BDS-3/GPS PPP time transfers in Scheme1 can realize about 0.2 ns accuracy. When the new clock model is applied, the accuracy can be improved by up to 45% and 39.8% for BDS-3 and BDS-3/GPS PPP, respectively. The proposed clock model can significantly improve the short-term frequency stability by 57.4%, but less for the long-term stability.

Keywords PPP-B2b, BDS-3, Time transfer, Receiver clock model

Introduction

Global Navigation Satellite System (GNSS) is an indispensable tool for timing or time transfer due to its continuity and high-precision (Defraigne & Petit, 2003; Levine, 2008; Vondrák, 1969). Timing is one of the important applications of BeiDou Navigation Satellite System (BDS) (Yang et al., 2011). Since July 2020 BeiDou-3 Navigation Satellite System has officially started its global Positioning, Navigation, and Timing (PNT) service, which opens up more application opportunities (Xiao et al., 2022; Yang et al., 2019, 2020). Based on BDS-3, the studies on high-precision positioning (Shi et al., 2020; Zhao et al., 2021), bias estimation (Li et al., 2022), orbit determination (Zhao et al., 2022), and time transfer (Xiao et al., 2021) were conducted.

The Global Positioning System (GPS) All-in-View (AV) and Common-View (CV) techniques with pseudorange observations have been used for time transfer (Peng 2004; Petit and Jiang 2008a). To achieve a higher time transfer accuracy, carrier phase measurements are adopted. Nowadays, Precise Point Positioning (PPP) is one of the main time transfer technologies using carrier phase measurements (Defraigne 2007) and has been formally applied to the International Atomic Time (TAI) comparison since

*Correspondence:
Qing Wang
wq_seu@seu.edu.cn
[1] School of Marine Science and Engineering, Nanjing Normal University, Nanjing 210023, China
[2] School of Instrument Science and Engineering, Southeast University, Nanjing 211189, China
[3] Jiangsu Province Institute of Surveying and Mapping Engineering, Nanjing 210013, China
[4] College of Electronic Engineering, National University of Defense Technology, Hefei 230037, China
[5] School of Geography, Nanjing Normal University, Nanjing 210023, China
[6] Faculty of Architecture, Civil, and Transportation Engineering, Beijing University of Technology, Beijing 100124, China
[7] State Key Laboratory of Geodesy and Earth's Dynamics, Innovation Academy for Precision Measurement Science and Technology, CAS, Wuhan 430077, China
[8] GNSS Research Center, Wuhan University, Wuhan 430079, China

2008 (Petit and Jiang 2008b). Petit (2009) presented that GPS PPP could achieve an accuracy of 0.3 ns using the final products. Since then, multi-GNSS PPP time transfer has became a hot research topic. Tu et al. (2018) presented a BDS-2 triple-frequency PPP model for time transfer and concluded that the performance of triple-frequency PPP was identical to that of dual-frequency PPP. The PPP time transfer with multi-GNSS was investigated by Ge et al. (2019). They indicated that multi-GNSS could enhance the reliability of time transfer compared to a single system. Further, quad-frequency PPP time transfer using Galileo satellites was introduced by Zhang et al. (2020). They found that the reliability and redundancy of time transfer were improved with multi-frequency PPP. In addition, the time transfer with single-frequency PPP was presented by Wang et al. (2022) with sub-nanosecond level accuracy for various low-cost high-precision applications. However, the above studies on post-processing PPP cannot meet the requirements for real-time and high-precision time transfer. Ge et al. (2018) investigated the performance of GPS PPP time transfer with real-time products and proposed a clock model to improve the real-time PPP. The results suggested that the time transfer with real-time GPS PPP could achieve an accuracy of 0.5 ns. Further, Guo et al. (2019) introduced a one-way timing method with real-time PPP using GNSS time. Moreover, a one-way timing for Coordinated Universal Time (UTC) service was released by Wu et al. (2021) based on PPP technology with an accuracy at sub-nanosecond level. However, the previous studies on real-time PPP require the Internet to transmit correction information, which is difficult to ensure the reliability of time transfer. Fortunately, BDS-3 now provides the PPP-B2b service based on B2b signals for the Asia–Pacific region (CSNO, 2020a; Yang et al., 2020, 2022). Tao et al. (2021) assessed the BDS-3 PPP-B2b real-time stream as compared to that of Centre National d'Etudes Spatiales (CNES). Their results suggested that compared with GPS the PPP-B2b could have better availability than that of CNES for BDS-3 in Asia. Xu et al. (2021) indicated that BDS-3 PPP with the PPP-B2b could achieve the horizontal positioning accuracy of 11 cm and the vertical accuracy of 17 cm. Additionally, Zhang et al. (2022) carried out a preliminary analysis of PPP time transfer with the PPP-B2b correction and obtained the accuracy at the sub-nanosecond level. However, the receiver clock offset will absorb the unknown errors and noises in the real-time PPP (Chen et al., 2018; Zhang et al. 2015). Ge et al. (2019) presented a real-time PPP time transfer with a receiver clock model and concluded that the receiver clock model would improve the time transfer accuracy significantly. A receiver clock model was applied to PPP time transfer with International GNSS Service (IGS) final products by Lyu et al. (2019). The results show that the accuracy can be improved by about 18.3% for all time links. In addition, when the observations and the PPP-B2b corrections are abnormal, there exists a re-convergence problem. Therefore, a new clock model should be developed.

The paper is structured as follows. After the introduction, the method of the recovery of precise clock offset and orbit, time transfer with the PPP-B2b, and a receiver clock model are presented in the second section. The processing strategy and an experiment setup are introduced. The investigation and validation of the time transfer using the PPP-B2b correction without/with the clock model are followed. Finally, the findings of this research are summarized.

Methodology

In this part, the recovery of clock offset and orbit using the broadcast ephemeris and the PPP-B2b correction is presented. Then, the time transfer method with the PPP-B2b service is introduced in detail.

Recovery method of precise products from the PPP-B2b

Precise orbit is made up of the PPP-B2b correction and broadcast ephemeris (Xu et al., 2021), which is represented as

$$\begin{cases} \boldsymbol{X} = \boldsymbol{X}_{\mathrm{brd}} + (\boldsymbol{g}_r, \boldsymbol{g}_a, \boldsymbol{g}_c) \cdot \Delta \boldsymbol{O} \\ \Delta \boldsymbol{O} = [\Delta O_r, \Delta O_a, \Delta O_c] \\ \boldsymbol{g}_r = \dfrac{\boldsymbol{r}}{|\boldsymbol{r}|} \\ \boldsymbol{g}_c = \dfrac{\boldsymbol{r} \times \dot{\boldsymbol{r}}}{|\boldsymbol{r} \times \dot{\boldsymbol{r}}|} \\ \boldsymbol{g}_a = \boldsymbol{g}_c \times \boldsymbol{g}_r \end{cases} \tag{1}$$

where $\boldsymbol{X}$ is the vector of precise orbit; $(\boldsymbol{g}_r, \boldsymbol{g}_a, \boldsymbol{g}_c)$ indicates the transformation matrix in Radial, Along, and Cross (RAC) direction; $\boldsymbol{X}_{\mathrm{brd}}$ is the satellite orbits from broadcast ephemeris; $\Delta \boldsymbol{O}$ is the PPP-B2b correction in RAC direction; $\boldsymbol{r}$ and $\dot{\boldsymbol{r}}$ are the satellite position and velocity.

The precise clock can be recovered from the PPP-B2b correction and the satellite clock in broadcast ephemeris and is expressed as

$$T = T_{\mathrm{brd}} - \frac{\Delta T}{c} \tag{2}$$

where T indicates the recovered satellite clock; T_{brd} is the satellite clock in broadcast ephemeris; c is the speed of light; and ΔT is the clock correction.

PPP Time transfer method

A dual-frequency Ionosphere-Free (IF) PPP is used for time transfer (Petit and Jiang 2008b). After applying precise products and corresponding correction models

(Zumberge et al., 1997), the code and carrier phase observations read as

$$p^s_{r,\mathrm{IF}^{ij}} = \mathbf{e}^s_r \cdot \Delta(x,y,z) + c\mathrm{d}\bar{t}_{r,\mathrm{IF}^{ij}} + M^s_{r,w} \cdot Z_w + \xi^s_{r,\mathrm{IF}^{ij}} \tag{3}$$

$$l^s_{r,\mathrm{IF}^{ij}} = \boldsymbol{\mu}^s_r \cdot \Delta(x,y,z) + c\mathrm{d}\bar{t}_{r,\mathrm{IF}^{ij}} + M^s_{r,w} \cdot Z_w + N^s_{r,\mathrm{IF}^{ij}} + \psi^s_{r,\mathrm{IF}^{ij}} \tag{4}$$

where $p^s_{r,\mathrm{IF}^{ij}}$ and $l^s_{r,\mathrm{IF}^{ij}}$ are the IF pseudorange and carrier phase observations after correcting the corresponding errors; $\mathbf{e}^s_r$ is the linearized coefficient vector; s and r indicate the satellites and receiver; $\Delta(x,y,z)$ is the coordinate increment;$\boldsymbol{\mu}^s_r$ indicates the vector of coefficient for coordinates; j and i indicate the frequency; $\mathrm{d}\bar{t}_{r,\mathrm{IF}^{ij}} = \mathrm{d}t_r + d_{\mathrm{IF}}$ illustrates the receiver clock offset, which includes hardware delay d_{IF}; $M^s_{r,w}$ demonstrates the wet mapping function; Z_w represents the tropospheric Zenith Wet Delay (ZWD); $N^s_{r,\mathrm{IF}^{ij}}$ is the float IF ambiguity, $\psi^s_{r,\mathrm{IF}^{ij}}$ and $\xi^s_{r,\mathrm{IF}^{ij}}$ are the observations noise.

Note that the reference for the BDS-3 satellite clock is the BDS Time (BDT), while the reference for the GPS clock is not the GNSS time in the PPP-B2b service. However, time transfer will eliminate the reference. After calibrating hardware delay $\mathrm{d}\bar{t}_{r,IF^{ij}}$, the difference d_u between local time and BDT, estimated from BDS-3 PPP with the PPP-B2b correction, can be expressed as

$$d_u = t_{\mathrm{local}} - t_{\mathrm{BDT}} \tag{5}$$

where u represents the user; and t_{local} indicates the local time. Note that the hardware delay is usually constant and varies little in a short term. Due to the complexity of hardware delay calibration, hardware delay calibration is not carried out in this contribution.

The time difference between the two different users Δt is represented as

$$\Delta t = d_1 - d_2 = d_1 - t_{\mathrm{BDT}} - (d_2 - t_{\mathrm{BDT}}) = t_1 - t_2 \tag{6}$$

where t_1 and t_2 are the local time at different stations.

Clock model

Usually, the receiver clock offset can be modeled as

$$x(t) = x_0 + y_0 t + \frac{1}{2}at^2 + \psi(t) \tag{7}$$

where $x(t)$ is the phase deviation; x_0 indicates the initial phase; y_0 is frequency deviation; a represents frequency aging factor; and $\psi(t)$ illustrates random noise of the clock.

For receiver clock modeling in PPP, the White Frequency-Modulated (WFM) noise, Flicker Frequency-Modulated (FFM) noise, and Random Walk Frequency-Modulated (RWFM) noise are usually considered. The relationship between Allan variance $\sigma^2_y(\tau)$ and clock noises can be expressed (Galleani & Tavella, 2003) as

$$\sigma^2_y(\tau) = h_{-2}\frac{(2\pi)^2}{6}\tau + h_{-1}2\log_e^2 + h_0\frac{1}{2\tau} \tag{8}$$

where h_{-2}, h_{-1} and h_0 are the coefficients of the RWFM, FFM, and WFM, respectively;τ is the sample interval.

In this contribution, the two-order clock model is employed and expressed as

$$\begin{bmatrix} x_1(k+1) \\ x_2(k+1) \end{bmatrix} = \begin{bmatrix} 1 & \tau \\ 0 & 1 \end{bmatrix} \begin{bmatrix} x_1(k) \\ x_2(k) \end{bmatrix} + \begin{bmatrix} w_1(\tau) + \int_{k\tau}^{k\tau+\tau} w_2(u)\mathrm{d}u \\ w_2(\tau) \end{bmatrix} \tag{9}$$

where $x_1(k)$ is the receiver clock offset at the k epoch; $x_2(k)$ denotes part of the frequency deviation at the k epoch, including the systematic term and the RWFM in the random term; Random walk frequency noise appears as a Wiener process in the frequency dimension of the discrete model, denoted as $w_2(\tau)$ and in the dimension of clock offset it appears as an integral of the Wiener process, denoted as $\int_{k\tau}^{k\tau+\tau} w_2(u)\mathrm{d}u$; $w_1(\tau)$ is the WFM.

The above clock model does not consider the FFM. For high-performance atomic clocks, the FFM is relatively low and can be neglected. However, for low-cost crystal oscillators, such as constant temperature crystal oscillators, the FFM is ubiquitous and has good performance in short-term stability. If FFM is not considered in modeling, the model accuracy will be reduced. In this work, the Kalman filter is used for estimating parameters. Based on the clock model (Eq. 8), the FFM components are added to the noise covariance matrix $\boldsymbol{Q}$, which can be expressed as

$$\boldsymbol{Q} = \begin{bmatrix} \frac{1}{2}h_0 + 2h_{-1}\tau^2 + \frac{2\pi^2}{3}h_{-2}\tau^3 & \pi^2 h_{-2}\tau^2 \\ \pi^2 h_{-2}\tau^2 & 2\pi^2 h_{-2}\tau \end{bmatrix} \tag{10}$$

Note that the coefficients of the RWFM, FFM, and WFM can be estimated with the least squares method with the Allan deviation.

The processing of the receiver clock model includes the following steps. First, we use the white noise model to estimate the receiver clock offset of the station with the final products, and 15 consecutive days of the observation data are used in our work; Second, we use Stable 32 software (http://www.wriley.com/) to calculate the Allan variance. Third, the least squares method and formula (8) are applied to estimate the corresponding coefficients. It is not necessary to estimate these coefficients every time, but only once over a period of time, such as one year. Finally, we put the coefficients into the formula (10) and estimate the receiver clock

offset by combining the formulas (3), (4), (7), (9), and (10).

In addition, based on the elevation-dependent weighting, the precisions of orbit and clock calculated from the PPP-B2b correction also need to be considered. The weight $\boldsymbol{W}$ can be expressed as

$$\begin{cases} \boldsymbol{W} = \mathrm{diag}(\sigma_1^{-2}, \sigma_2^{-2}, \sigma_3^{-2}, \ldots, \sigma_m^{-2}) \\ \sigma^2 = FR_r(a_\sigma^2 + b_\sigma^2 \Big/ \sin E^2) + \sigma_{\mathrm{eph}}^2 \end{cases} \tag{11}$$

where F is the satellite systematic error factor (GPS: BDS-3 = 1:1). R_r indicates code/carrier phase error ratio (10 000). a_σ and b_σ are carrier-phase error factors 0.006 and 0.01 (m). E illustrates elevation angle. σ_{eph} is the URA from the PPP-B2b service, and m is the number of satellites.

Experimental setups

To evaluate the efficiency of the new clock model in PPP time transfer with the PPP-B2b service, one station from a timing lab and two stations from the Multi-GNSS Experiment (MGEX) were selected. The processing strategy is discussed in this section.

Dataset

Only two MGEX stations (CUSV and USUD) and one station (TLM2) in the timing lab were selected for this work because of very few stations equipped with the atomic clock in Asia. They are shown in Fig. 1. Here, USUD is connected to an H-master clock, while the frequency signal of station CUSV is provided with a high-performance crystal oscillator. The observations, broadcast ephemeris, and the PPP-B2b correction were received from Day of the Year (DOY) 68 to 72, 2022. Additionally, GPS PPP with IGS final products was calculated to assess PPP time transfer with the PPP-B2b correction. Note that the five days of observations were processed consecutively.

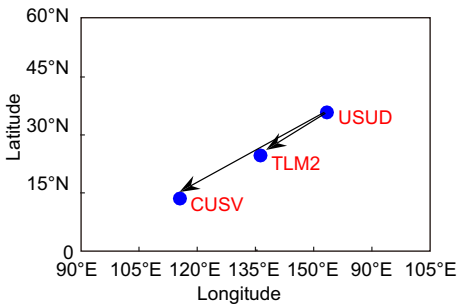

Fig. 1 CUSV and USUD stations were selected from MGEX. TLM2 was selected from a timing lab. All selected stations can be covered by the PPP-B2B service

Processing strategy

The dual-frequency PPP method is used in this contribution. The detailed processing strategy of real-time PPP for time transfer is listed in Table 1. The errors that can be corrected directly with the models, such as Sagnac effect, relativistic effects et al., are corrected using the IERS standard models (Petit & Luzum, 2010). Two schemes are utilized in this contribution. First, the receiver clock offset is estimated as the white noise in BDS-3, GPS, and BDS-3/GPS PPP, which is called Scheme 1. Second, the receiver clock offset is handled using the clock model in our work for BDS-3 and BDS-3/GPS PPP, which is called Scheme 2. In addition, for BDS-3/GPS PPP, an Inter-System Bias (ISB) parameter is added. Here, the receiver clock offset is set to BDS-3 observations, whilst the receiver clock offset of GPS observations consists of the receiver clock offset of BDS-3 and ISB. Because the quality of GPS in the PPP-B2b correction is poorer than that of BDS-3 (Tao et al., 2021), the GPS PPP using IGS final products is set as the time standard.

Results and validation

In this section, GPS, BDS-3, and BDS-/GPS PPP time transfer results are presented and compared with each other (Scheme 1). Then, real-time PPP using the newly developed clock model is further studied (Scheme 2).

GPS, BDS-3, and BDS-3/GPS PPP without the clock model

The receiver clock offsets at stations CUSC, USUD, and TLM2 estimated with GPS, BDS-3, and BDS-3/GPS PPP with the PPP-B2b correction are displayed in Fig. 2. From three figures, we can draw some initial conclusions. First, the receiver clock offset with GPS PPP shows disordered

Table 1 Information on PPP time transfer with the PPP-B2b correction

Estimator	Kalman
Signals	GPS: L1/L2 BDS-3: B1C/B2a
Phase Center Variation (PCV) and Phase Center Offset (PCO)	"Atx" file
Receiver clock offset	White noise (Scheme 1)
	The clock model (Scheme 2)
Precise products	Broadcast ephemeris (CNAV1 or LNAV) + PPP-B2b correction
	IGS final products
Tropospheric delay	ZHD: corrected (Saastamoinen, 1972)
	ZWD: estimated
Tidal displacement	Corrected
Phase ambiguities	Estimate as constant
Receiver coordinates	Estimate as constant

fluctuations and even many outliers. As we know, the receiver clock offsets consist of the difference between the local time and the reference time, hardware delay, and other noise. Hence, the fluctuations in the results are mainly caused by the reference time of GPS in the PPP-B2b service, which was introduced in Subsect. 2.2. In addition, due to the continuity of data or products and the small number of available satellites in some time periods, the solution for the clock offset parameter of the receiver needs re-converging, leading to receiver clock offset jumps. On the contrary, the receiver clock offsets of BDS-3 PPP at all stations are smooth and continuous. This is understandable because the reference time of BDS-3 is BDT in the PPP-B2b service (CSNO, 2020b). Here, we suggest that the clock model is not suitable for GPS PPP because the receiver clock offset is random and difficult to model. Therefore, the clock model was applied to BDS-3 PPP or BDS-3/GPS PPP time transfer. The second finding is that the receiver clock offsets at all stations have different characteristics. When the reference time of products is the same for the receiver measurements, the different characteristics of receiver clock offsets are determined by the receiver clock. The performance of the clock connected to TLM2 is the best among the three stations because it is more stable and drifts less. Third, the results of GPS PPP have an obvious interruption phenomenon for all stations. This is due to less than four satellites used at that station for some time. Luckily, real-time BDS-3 PPP doesn't have that phenomenon. Fourth, the tendency of BDS-3 PPP is almost identical to that of BDS-3/GPS in terms of the trend and the value of the receiver clock offsets for three stations.

Figures 3, 4, and 5 show the clock differences of CUSV-USUD and TLM2-USUD obtained from GPS, BDS-3, and BDS-3/GPS real-time PPP with the PPP-B2b correction, respectively. An obvious phenomenon can be found in Fig. 3. There are obvious interruptions in the clock difference time series and apparent outliers in the time series of TLM2-USUD, which further confirms the above conclusion that the receiver clock in the GPS PPP with the PPP-B2b correction is not suitable for modeling. Another finding is that the GPS PPP time transfer of TLM2-USUD performs worse than BDS-3 PPP. In addition, the GPS PPP solution has a lot of discontinuities in both CUSV-USUD and TLM2-USUD time series. Therefore, we do not recommend the time transfer using GPS -only PPP with the PPP-B2b service. Luckily, the BDS-3 or BDS-3/GPS PPP time transfer is highly recommended using the PPP-B2b service, as illustrated in Figs. 4, and 5, both presenting a continuous and stable time series.

To quantify our previous conclusion and verify the performance of time transfer with the PPP-B2b correction,

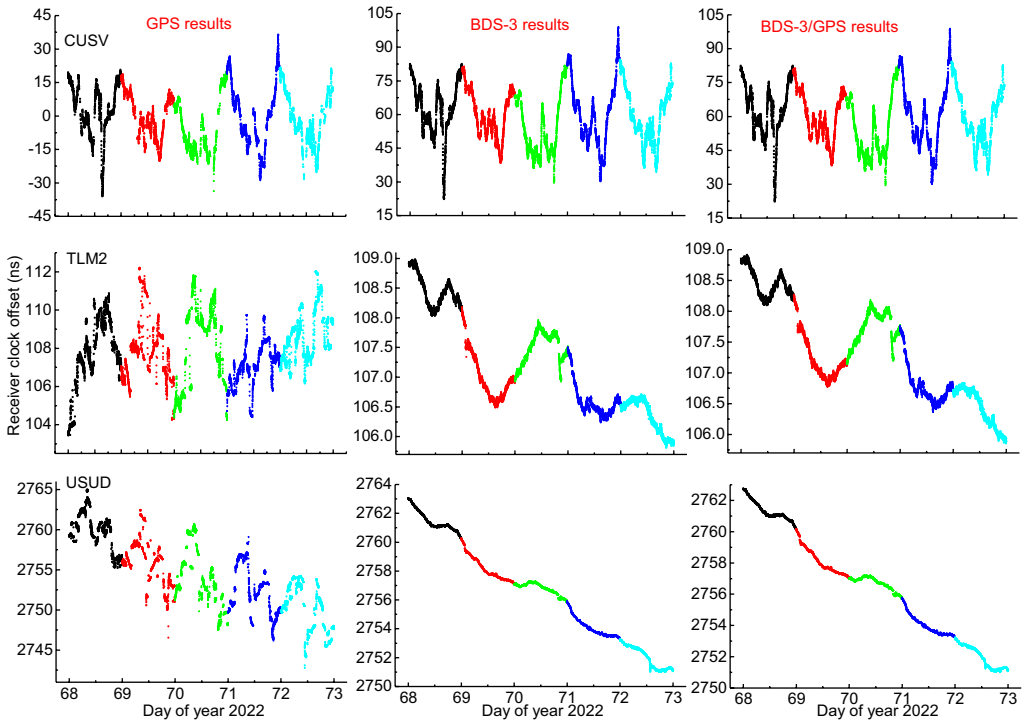

Fig. 2 Receiver clock offsets of CUSV, TLM2, and USUD stations from GPS, BDS-3, or BDS-3/GPS PPP in Scheme1. Different colors indicate the results of different days

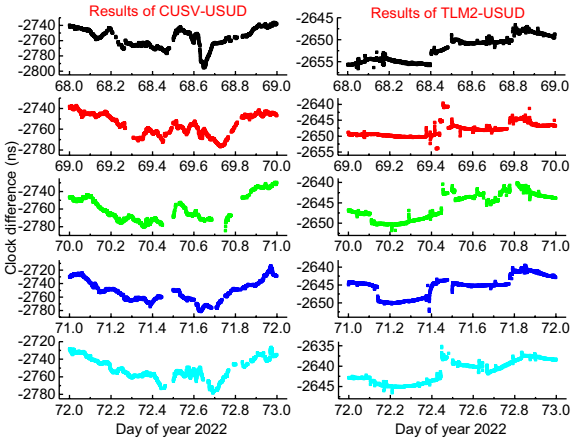

Fig. 3 Clock differences of CUSV-USUD and TLM2-USUD from GPS PPP in Scheme 1

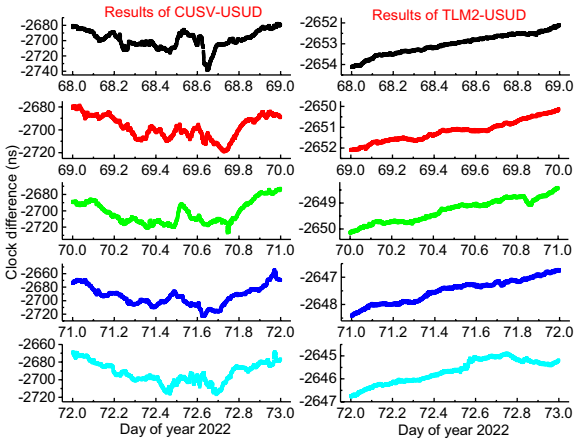

Fig. 4 Clock differences of CUSV-USUD and TLM2-USUD from BDS-3 PPP in Scheme1

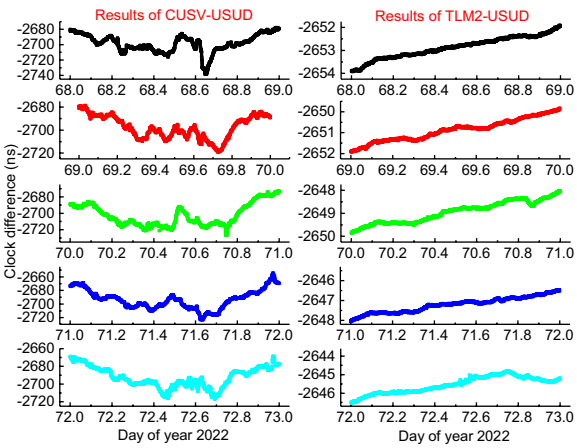

Fig. 5 Clock differences of CUSV-USUD and TLM2-USUD from BDS-3/GPS PPP in Scheme 1

we calculated the mean values (Mean) and Standard Deviation (STD) values of clock difference between PPP time transfer with the PPP-B2b correction and that of IGS final products and present them in Table 2. We can find some interesting conclusions from the numerical results. The first is that an obvious systematic bias between GPS and BDS-3 PPP time transfer solutions exists. The possible reason is that the hardware delay is different for different frequencies at the receiver end. The second is that the mean values of BDS-3 are almost equal to that of BDS-3/GPS with the PPP-B2b correction. The third is the STD values of the clock difference are about 1–2 ns for GPS PPP, which supports the previous conclusion that GPS PPP using the PPP-B2b correction is not suitable for time transfer. The fourth is that the BDS-3 PPP time transfer accuracy is about 0.2 ns for all time series using the PPP-B2b correction. In addition, the improvement of BDS3/GPS with respect to the BDS-3 PPP time transfer is very limited. There are three possible reasons for the above phenomenon: (1) the qualities of the products recovered from the PPP-B2b correction were much worse than that of BDS-3 satellites; (2) very fewer GPS satellites were used. Fig. 6 shows the number of satellites used on DOY 68, 2022; (3) The User Range Error (URE) in the PPP-B2b service was added to the weight of each satellite. In addition, we can see that there are some epochs when the number of used GPS satellites is small in the PPP processing. Unlike final precise products, the PPP-B2b service does not provide the orbit and clock corrections for all GPS satellites at any given moment. Moreover, some GPS satellites were excluded due to their large residuals. After the filter update, we check the observation residuals for each satellite. If the residual of a satellite exceeds some torelance, the weight of this abnormal observation is reduced, and the filter restarts. If the result is still not satisfied, we will further eliminate the satellites with too large residuals.

To further analyze PPP time transfer using the PPP-B2b service from the frequency domain, we calculated the Modified Allan Deviation (MDEV) of CUSV-USUD and TLM2-USUD time links and display them in Fig. 7, respectively. The mean MDEV of CUSV-USUD obtained from BDS-3, GPS, and BDS-3/GPS PPP is about 2.56×10^{-12}, 2.24×10^{-12}, and 2.23×10^{-12} at 960 s. In addition, the mean MDEV of TLM2-USUD is about 1.86×10^{-13}, 3.12×10^{-14}, and 3.05×10^{-14} at 960 s. In terms of short-term frequency stability, GPS PPP is much worse than BPS-3 PPP, especially for the TLM2-USUD, and the improvement by including GPS satellites to BDS-3 PPP is limited with the PPP-B2b correction, which is similar to the above conclusion. Besides, the long-term frequency stability also shows a similar characteristic with (8.53×10^{-13}, 7.68×10^{-13}, 7.61×10^{-13})

Table 2 Mean and STD values of the difference between the time transfer solutions calculated from BDS-3, GPS, and BDS-3/GPS PPP in Scheme 1 and the PPP time transfer with IGS final products (ns)

Time-link	DOY	Results of GPS		Results of BDS-3		Results of BDS-3/GPS	
		Mean	STD	Mean	STD	Mean	STD
CUSV-USUD	68	−4.35	1.12	53.92	0.13	54.04	0.11
	69	−3.67	1.03	54.4	0.18	54.38	0.17
	70	−3.83	1.24	54.44	0.16	54.4	0.14
	71	−4.29	1.56	54.5	0.14	54.46	0.13
	72	−4.66	1.02	54.6	0.15	54.51	0.14
TLM2-USUD	68	2.26	2.05	1.51	0.15	1.66	0.13
	69	4.77	1.28	1.78	0.12	1.80	0.10
	70	5.42	2.48	2.08	0.1	2.01	0.09
	71	4.36	2.27	2.17	0.19	2.05	0.17
	72	6.21	2.03	2.1	0.2	2.04	0.18

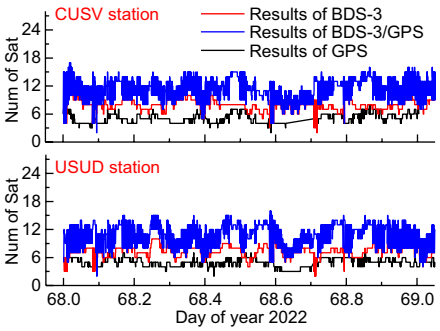

Fig. 6 Number of satellites used in the PPP processing for CUSV and USUD stations on DOY 68, 2022

for CUSV-USUD and $(5.92 \times 10^{-14}, 8.56 \times 10^{-15}, 7.77 \times 10^{-15})$ for TLM2-USUD for GPS, BDS-3, and BDS-3/GPS time transfer using the PPP-B2b service.

BDS-3 and BDS-3/GPS PPP with/without the clock model

As we pointed out earlier, GPS PPP with the PPP-B2b correction is not suitable for modeling. Hence, BDS-3/GPS or BDS-3 PPP time transfer using the PPP-B2b correction with/without the clock model was studied. The receiver clock offsets at CUSV, USUD, and TLM2 estimated from BDS-3 PPP using the PPP-B2b correction with/without the clock model are displayed in Figs. 8

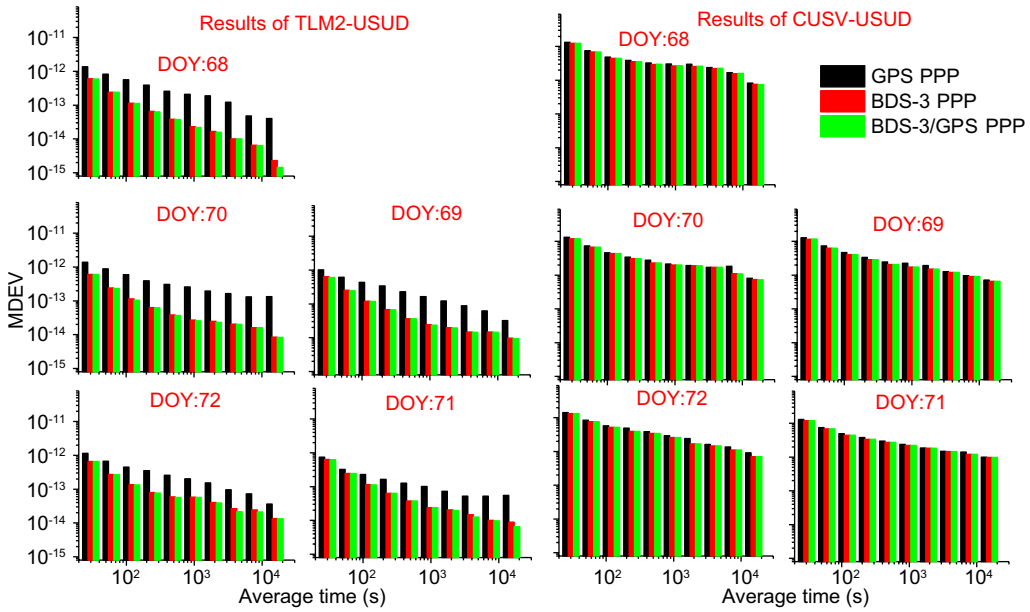

Fig. 7 MDEV of CUSV-USUD and CUSV-USUD from BDS-3, GPS, and BDS-3/GPS PPP in Scheme 1

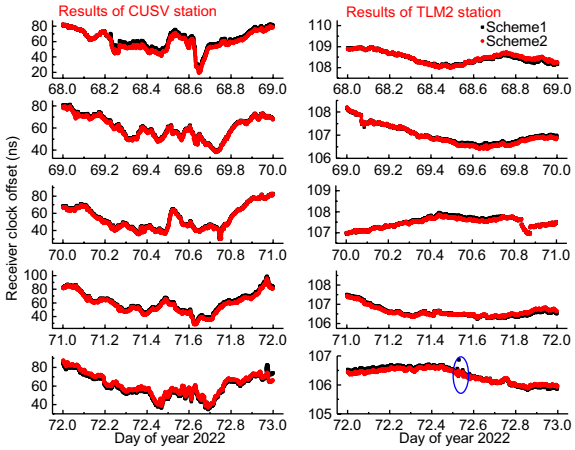

Fig. 8 CUSV and TLM2 receiver clock offsets from BDS-3 PPP in Scheme 1 and Scheme 2

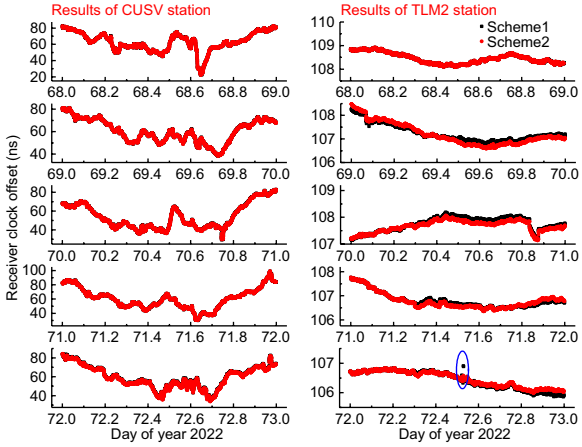

Fig. 10 CUSV and TLM2 receiver clock offsets from BDS-3/GPS PPP in Scheme 1 and Scheme 2

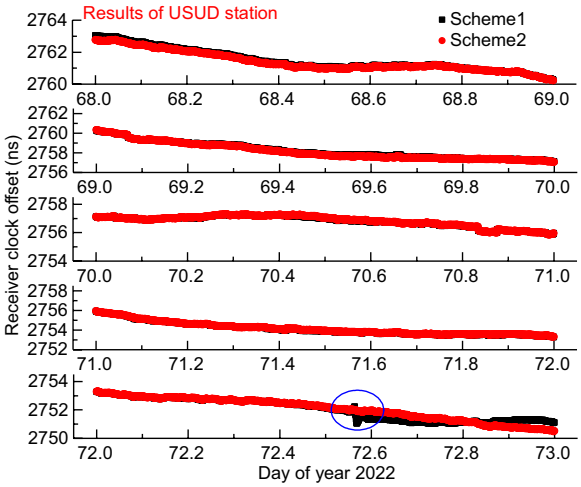

Fig. 9 USUD receiver clock offsets from BDS-3 PPP in Scheme 1 and Scheme 2

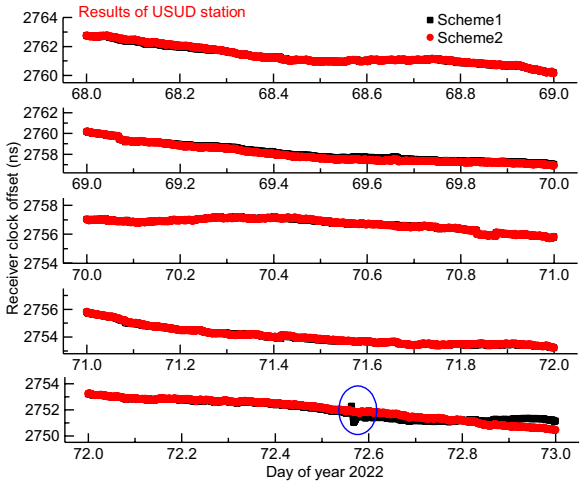

Fig. 11 USUD receiver clock offsets from BDS-3/GPS PPP in Scheme 1 and Scheme 2

and 9. In addition, the receiver clock offsets from BDS-3/GPS PPP with/without the clock model are displayed in Figs. 10 and 11. Three obvious conclusions can be found. The first is that the time series of Scheme 1 and Scheme 2 are in good agreement with each other without obvious systematic bias. The second is that the Scheme 2 can remove outliers with respect to Scheme 1, as seen in Figs. 8 and 10. The third is that Scheme 2 avoids the re-convergence of time transfer which is caused by data anomalies compared with Scheme 1, as seen from Figs. 9 and 11. The reconvergence phenomenon in Figs. 9 and 11 is mainly due to the short time interruption of the observed data at USUD station. If the interruption of observation data or PPP-B2B products lasts for more than 5 min, the corresponding parameters in the Kalman filter, such as ambiguity or receiver clock offset, will be reconfigured, resulting in obvious convergence of receiver clock offset. In addition, in some time periods very few satellites participate in PPP due to large residual errors will also lead to the anomaly of receiver clock offset. Overall, the advantage of the receiver clock model can predict the receiver clock offsets and constrain the equation at the next time when the data is abnormal.

Figures 12 and 13 exhibit the time transfer of CUSV-USUD and TLM2-USUD estimated from Scheme 1 and Scheme 2, respectively. From the figures, we can easily see that the time transfer solutions of Scheme 2 are smoother than those of Scheme 1, especially for the TLM2-USUD time series. Of course, the time transfer of Scheme 2 has obvious advantages over traditional methods in eliminating outliers and avoiding reconvergence,

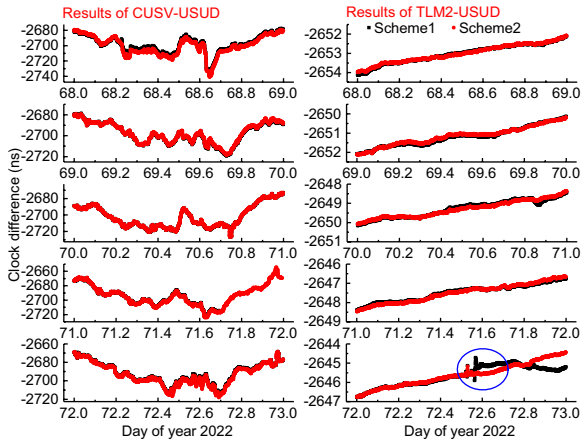

Fig. 12 Clock difference of CUSV-USUD and TLM2-USUD from BDS-3 PPP in Scheme 1 and Scheme 2

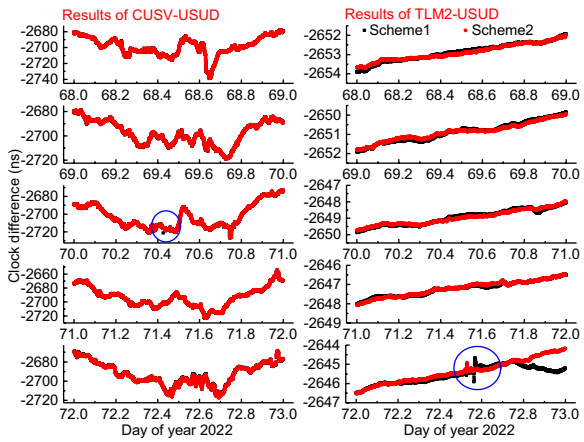

Fig. 13 Clock difference of CUSV-USUD and TLM2-USUD from BDS-3/GPS PPP in Scheme 1 and Scheme 2

as seen in Figs. 12 and 13. We further analyze the performance of the two schemes. The STD and mean values of the clock difference are given in Table 3. We found that the improvement of time transfer by the clock model is obvious. Both BDS-3 and BDS-3/GPS PPP with the PPP-B2b correction can achieve a time transfer accuracy of better than 0.2 ns, BDS-3/GPS PPP even reaches about 0.1 ns. For BDS-3 PPP, the improvement percentage of Scheme 2 ranges from 14.3% to 45% compared to Scheme 1, especially for PPP time transfer under reconvergence. In addition, the BDS-3/GPS time transfer accuracy is enhanced wih the clock model by 7.14% to 38.89%, which further proves the superiority of the clock model.

For frequency stability, a similar conclusion can be drawn. The MDEV of CUSV-USUD and TLM2-USUD with BDS-3 or BDS-3/GPS PPP with/without the clock model is exhibited in Figs. 14 and 15. An interesting finding is that TLM2-USUD outperforms CUSV-USUD. The reason is that the atomic clock connected to TLM2 has better performance than that of CUSV, because the frequency signal of CUSV mainly comes from the high-performance crystal oscillator. Furthermore, the improvement of Scheme 2 is obvious as compared to Scheme 1. For BDS-3 PPP, the mean MDEV of CUSV-USUD is $(2.25 \times 10^{-12}, 2.15 \times 10^{-12})$ and that of TLM2-USUD is $(3.10 \times 10^{-14}, 2.36 \times 10^{-14})$ for Scheme 1 and Scheme 2 at 960 s. The mean MDEV of TLM2-USUD is $(7.64 \times 10^{-13}, 7.14 \times 10^{-13})$ and that of TLM2-USUD is $(8.56 \times 10^{-15}, 6.85 \times 10^{-15})$ for Scheme 1 and Scheme 2 at 15 360 s. For BDS-3/GPS PPP, the mean MDEV of CUSV-USUD is $(2.25 \times 10^{-12}, 2.15 \times 10^{-12})$ and that of TLM2-USUD is $(3.10 \times 10^{-14}, 2.32 \times 10^{-14})$ for Scheme 1 and Scheme 2 at 960 s. The mean MDEV of CUSV-USUD is $(7.61 \times 10^{-13}, 7.20 \times 10^{-13})$ and that of TLM2-USUD is $(7.77 \times 10^{-15}, 5.84 \times 10^{-15})$ for Scheme 1 and Scheme 2 at 15 360 s. In addition, the improvement of Scheme 2 relative to Scheme 1 is plotted in Fig. 16. For BDS-3 PPP, the greatest improvement is about 45.9% and 56.6% for CUSV-USUD and TLM2-USUD time links, respectively. For BDS-3/GPS PPP, the largest improvement of Scheme 2 is approximately 45.8% and 57.4% for CUSV-USUD and TLM2-USUD time links. More interestingly, the short-term frequency stability improved significantly, but less for the long-term frequency stability by the clock model for two time-links except for time transfer solutions on DOY 72 for TLM2-USUD. It proves that the clock model can avoid the receiver clock from absorbing excess noise. Both the short- and long-term frequency stability will be improved significantly with the clock model when the data is abnormal, which can be proved by the TLM2-USUD on DOY 72. Overall, the clock model can enhance BDS-3 or BDS-3/GPS PPP time transfer using the PPP-B2b service.

Summary

BDS-3's characteristic service, the PPP-B2b service, can be used for high-quality PNT services in the Asia–Pacific region without the Internet, which brings new opportunities for PPP time transfer. However, the traditional PPP method cannot solve the problem that the receiver clock offsets absorb the excess noise and need the re-convergence of the solution when there exist abnormal data. To enhance PPP time transfer with the PPP-B2b correction, we proposed a clock model and verified its reliability, feasibility, and superiority with an experiment using 5 consecutive days of data at three stations.

The traditional PPP time transfer method using BDS-3, GPS, and BDS-3/GPS satellites with the PPP-B2b correction was tested. The results suggested that GPS time transfer with the PPP-B2b is not recommended because

Table 3 Mean and STD of the difference between the time transfer solutions calculated from BDS-3 and BDS-3/GPS PPP in Scheme 1 and Scheme 2 (ns) and the PPP time transfer with IGS final products. Note that (%) indicates the improvement of Scheme 2 compared to Scheme 1 for the STD values

Time-links	DOY	Results of BDS-3				Improvement (%)	Results of BDS-3/GPS				Improvement (%)
		Scheme 1		Scheme 2			Scheme 1		Scheme 2		
		Mean	STD	Mean	STD		Mean	STD	Mean	STD	
CUSV-USUD	68	53.92	0.13	53.42	0.11	15.38	54.04	0.11	54	0.1	9.09
	69	54.4	0.18	54.82	0.14	22.22	54.38	0.17	54.48	0.12	29.41
	70	54.44	0.16	54.87	0.13	18.75	54.4	0.14	54.38	0.12	14.29
	71	54.5	0.14	54.76	0.12	14.29	54.46	0.13	54.6	0.12	7.69
	72	54.6	0.15	54.86	0.11	26.67	54.51	0.14	54.2	0.13	7.14
TLM2-USUD	68	1.51	0.15	1.37	0.12	20.00	1.66	0.13	1.54	0.09	30.77
	69	1.78	0.12	1.72	0.1	16.67	1.80	0.1	1.8	0.08	20.00
	70	2.08	0.1	2.07	0.08	20.00	2.01	0.09	2.02	0.08	11.11
	71	2.17	0.19	2.07	0.15	21.05	2.05	0.17	2.12	0.12	29.41
	72	2.1	0.2	2.13	0.11	45.00	2.04	0.18	2.18	0.11	38.89

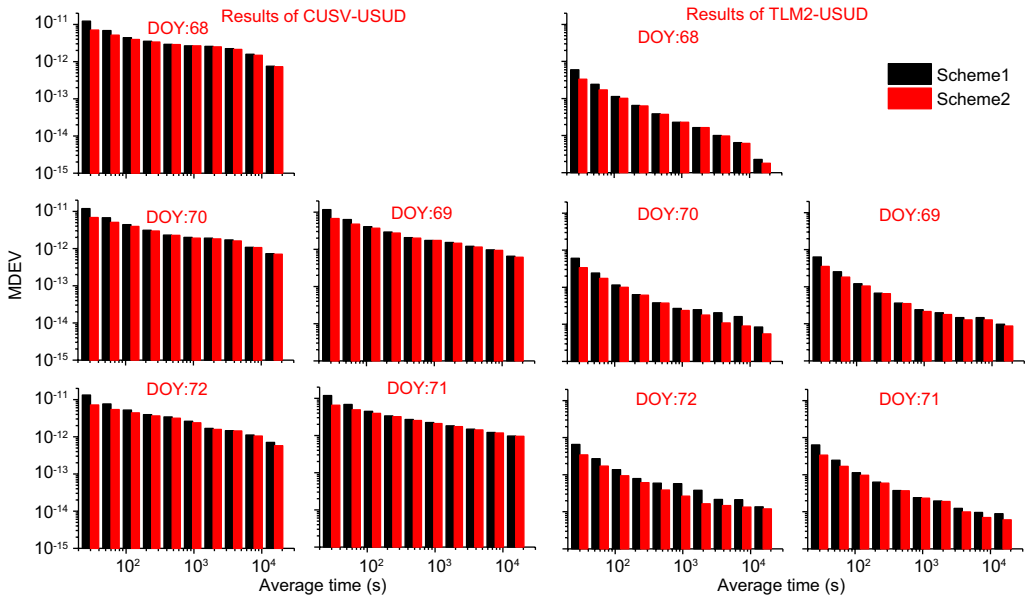

Fig. 14 MDEV of CUSV-USUD and TLM2-USUD from BDS-3 PPP Scheme 1 and Scheme 2

of low accuracy at 1–2 ns level. However, BDS-3 PPP time transfer using the PPP-B2b correction can achieve about accuracy of 0.2 ns. In addition, compared to BDS-3 PPP, the BDS-3/GPS PPP has less improvement. For frequency stability, the mean MDEV of TLM2-USUD is about (1.86×10^{-13}, 3.12×10^{-14}, 3.05×10^{-14}) at 960 s and (5.92×10^{-14}, 8.56×10^{-15}, 7.77×10^{-15}) at 15,360 s for BDS-3, GPS, and BDS-3/GPS time transfer with the PPP-B2b service.

Compared to the traditional PPP using the PPP-B2b service, the PPP with the new clock model has apparent advantages: (1) BDS-3 or BDS-3/GPS PPP time transfer can reach accuracy at 0.1 ns level. The greatest improvement percentage is about 45.0% and 38.9% for BDS-3 and BDS-3/GPS PPP, respectively; (2) the clock model can avoid a need for solution re-convergence when data is abnormal; (3) the clock model can significantly improve the short-term stability by up to 57.4%, but less for the long-term stability; (4) Both the long- and short-term frequency stability are much improved when there exist abnormal data.

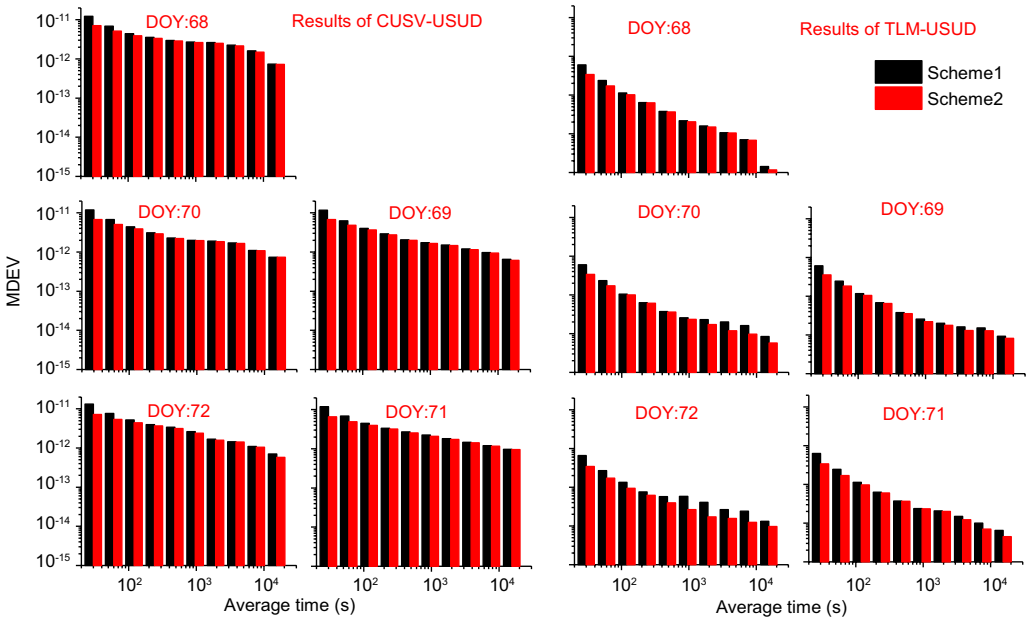

Fig. 15 MDEV of CUSV-USUD and TLM2-USUD from BDS-3/GPS PPP in Scheme 1 and Scheme 2

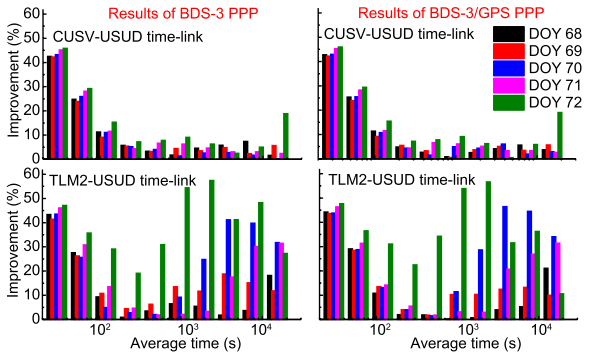

Fig. 16 The improvement of BDS-3 or BDS-3/GPS PPP with Scheme 2 with respect to that of Scheme 1 for two time-links (CUSV-USUD and TLM2-USUD)

Acknowledgements
Not applicable.

Author contributions
YG: original draft, review & editing the manuscript. QW, YW, FS, XM: review, editing. DL and XC: data procession. All authors read and approved the final manuscript. All authors read and approved the final manuscript.

Funding
This work was supported by the National Natural Science Foundation of China (Nos. 42104014; 42077003; 41904018). Natural Science Foundation of the Higher Education Institutions of Jiangsu Province, China (21KJB420005), State Key Laboratory of Geodesy and Earth's Dynamics (SKLGED2022-3-6) and High-level innovation and entrepreneurship talent plan of Jiangsu Province.

Availability of data and materials
The BDS tracking data are publicly available from IGS data centers, the PPP-B2b correction can be received from BDS-3.

Declarations

Competing interests
The author(s) declare(s) that they have no competing interests.

Received: 28 October 2022 Accepted: 12 February 2023
Published online: 06 March 2023

References

Chen, X., Lu, C., Guo, B., Guo, F., Ge, M., Li, X., & Schuh, H. (2018). GPS/GLONASS combined precise point positioning with the modeling of highly stable receiver clock in the application of monitoring active seismic deformation. *Journal of Geophysical Research: Solid Earth, 123*(5), 4025–4040. https://doi.org/10.1029/2017jb015060

CSNO (2020a) BeiDou navigation satellite system signal in space interface control document open service signal B2b (Version 1.0).

CSNO (2020b) BeiDou navigation satellite system signal in space interface control document precise point positioning service signal PPP-B2b (Version 1.0).

Defraigne, P., Carine, B., and Nicolas, G. (2007) PPP and phase-only GPS time and frequency transfer. In: Proceedings of the IEEE international frequency control symposium jointly with the 21st European frequency and time forum (EFTF '07), pp. 904–908.

Defraigne, P., & Petit, G. (2003). Time transfer to TAI using geodetic receivers. *Metrologia, 40*(4), 184–188. https://doi.org/10.1088/0026-1394/40/4/307

Galleani, L., & Tavella, P. (2003). On the use of the Kalman filter in timescales. *Metrologia, 40*(3), S326–S334. https://doi.org/10.1088/0026-1394/40/3/312

Ge, Y., Zhou, F., Liu, T., Qin, W., Wang, S., & Yang, X. (2018). Enhancing real-time precise point positioning time and frequency transfer with receiver clock modeling. *GPS Solutions*. https://doi.org/10.1007/s10291-018-0814-y

Ge, Y., Dai, P., Qin, W., Yang, X., Zhou, F., Wang, S., & Zhao, X. (2019). Performance of multi-GNSS precise point positioning time and frequency transfer with clock modeling. *Remote Sensing, 11*(3), 347. https://doi.org/10.3390/rs11030347

Guo, W., Song, W., Niu, X., Lou, Y., Gu, S., Zhang, S., & Shi, C. (2019). Foundation and performance evaluation of real-time GNSS high-precision one-way timing system. *GPS Solutions*. https://doi.org/10.1007/s10291-018-0811-1
Levine, J. (2008). A review of time and frequency transfer methods. *Metrologia, 45*(6), S162–S174. https://doi.org/10.1088/0026-1394/45/6/s22
Li, X., Li, X., Jiang, Z., Xia, C., Shen, Z., & Wu, J. (2022). A unified model of GNSS phase/code bias calibration for PPP ambiguity resolution with GPS, BDS, Galileo and GLONASS multi-frequency observations. *GPS Solutions*. https://doi.org/10.1007/s10291-022-01269-5
Lyu, D., Zeng, F., Ouyang, X., & Yu, H. (2019). Enhancing multi-GNSS time and frequency transfer using a refined stochastic model of a receiver clock. *Measurement Science and Technology*. https://doi.org/10.1088/1361-6501/ab2419
Peng, H.M., & Liao, C. S. (2004) GPS smoothed P3 code for time transfer. In: 18th European frequency and time forum, EFTF 2004. (pp. 137–141). IET.
Petit, G., Luzum, B., (2010) IERS conventions (2010) Bureau International Des Poids et Mesures Sevres (France). (No. IERS-TN-36).
Petit, G., & Jiang, Z. (2008). Precise point positioning for TAI computation. *International Journal of Navigation and Observation, 1*, 1–8. https://doi.org/10.1155/2008/562878
Petit, G., & Jiang, Z. (2008). GPS All in View time transfer for TAI computation. *Metrologia, 45*(1), 35–45. https://doi.org/10.1088/0026-1394/45/1/006
Petit G (2009) The TAIPPP pilot experiment. In: IEEE international frequency control symposium, joint with the 22nd European frequency and time forum. (2009) vol 1-2, pp. 116-119.
Saastamoinen, J. (1972). Atmospheric correction for the troposphere and stratosphere in radio ranging satellites. *The Use of Artificial Satellites for Geodesy, 15*, 247–251. https://doi.org/10.1029/GM015p0247
Shi, J., Ouyang, C., Huang, Y., & Peng, W. (2020). Assessment of BDS-3 global positioning service: ephemeris, SPP, PPP, RTK, and new signal. *GPS Solutions*. https://doi.org/10.1007/s10291-020-00995-y
Tao, J., Liu, J., Hu, Z., Zhao, Q., Chen, G., & Ju, B. (2021). Initial assessment of the BDS-3 PPP-B2b RTS compared with the CNES RTS. *GPS Solutions*. https://doi.org/10.1007/s10291-021-01168-1
Tu, R., Zhang, P., Zhang, R., Liu, J., & Lu, X. (2018). Modeling and performance analysis of precise time transfer based on BDS triple-frequency uncombined observations. *Journal of Geodesy, 93*(6), 837–847. https://doi.org/10.1007/s00190-018-1206-3
Vondrák, J. (1969). A contribution to the problem of smoothing observational data. *Bulletin of the Astronomical Institutes of Czechoslovakia, 20*(6), 349–355.
Wang, S., Ge, Y., Meng, X., Shen, P., Wang, K., & Ke, F. (2022). Modelling and assessment of single-frequency PPP time transfer with BDS-3 B1I and B1C observations. *Remote Sensing*. https://doi.org/10.3390/rs14051146
Wu, M., Sun, B., Wang, Y., Zhang, Z., Su, H., & Yang, X. (2021). Sub-nanosecond one-way real-time time service system based on UTC. *GPS Solutions*. https://doi.org/10.1007/s10291-021-01089-z
Xiao, X., Shen, F., Lu, X., Shen, P., & Ge, Y. (2021). Performance of BDS-2/3, GPS, and Galileo time transfer with real-time single-frequency precise point positioning. *Remote Sensing*. https://doi.org/10.3390/rs13214192
Xiao, G., Liu, G., Ou, J., Zhou, C., He, Z., Chen, R., Guo, A., & Yang, Z. (2022). Real-time carrier observation quality control algorithm for precision orbit determination of LEO satellites. *GPS Solutions*. https://doi.org/10.1007/s10291-022-01286-4
Xiaohong, Z., Xinghan, C., & Fei, G. (2015). High-performance atomic clock modeling and its application in precise point positioning. *Aca Geodaetica Et Cartographica Sinica, 44*(4), 392–398. https://doi.org/10.11947/j.AGCS.2015.20140287
Xu, Y., Yang, Y., & Li, J. (2021). Performance evaluation of BDS-3 PPP-B2b precise point positioning service. *GPS Solutions*. https://doi.org/10.1007/s10291-021-01175-2
Yang, Y., Li, J., Xu, J., Tang, J., Guo, H., & He, H. (2011). Contribution of the compass satellite navigation system to global PNT users. *Chinese Science Bulletin, 56*(26), 2813–2819. https://doi.org/10.1007/s11434-011-4627-4
Yang, Y., Gao, W., Guo, S., Mao, Y., & Yang, Y. (2019). Introduction to BeiDou-3 navigation satellite system. *Navigation, 66*(1), 7–18. https://doi.org/10.1002/navi.291
Yang, Y., Mao, Y., & Sun, B. (2020). Basic performance and future developments of BeiDou global navigation satellite system. *Satellite Navigation*. https://doi.org/10.1186/s43020-019-0006-0
Yang, Y., Ding, Q., Gao, W., Li, J., Xu, Y., & Sun, B. (2022). Principle and performance of BDSBAS and PPP-B2b of BDS-3. *Satellite Navigation*. https://doi.org/10.1186/s43020-022-00066-2
Zhang, P., Tu, R., Gao, Y., Zhang, R., & Han, J. (2020). Performance of Galileo precise time and frequency transfer models using quad-frequency carrier phase observations. *GPS Solutions*. https://doi.org/10.1007/s10291-020-0955-7
Zhang, R., He, Z., Ma, L., Xiao, G., Guang, W., Ge, Y., Zhang, X., Zhang, J., Tang, J., & Li, X. (2022). Analysis of BDS-3 PPP-B2b positioning and time transfer service. *Remote Sensing*. https://doi.org/10.3390/rs14122769
Zhao, Q., Guo, J., Liu, S., Tao, J., Hu, Z., & Chen, G. (2021). A variant of raw observation approach for BDS/GNSS precise point positioning with fast integer ambiguity resolution. *Satellite Navigation*. https://doi.org/10.1186/s43020-021-00059-7
Zhao, Q., Guo, J., Wang, C., Lyu, Y., Xu, X., Yang, C., & Li, J. (2022). Precise orbit determination for BDS satellites. *Satellite Navigation*. https://doi.org/10.1186/s43020-021-00062-y
Zumberge, J. F., Heflin, M. B., Jefferson, D. C., Watkins, M. M., & Webb, F. H. (1997). Precise point positioning for the efficient and robust analysis of GPS data from large networks. *Journal of Geophysical Research, B3*(102), 5005–5017.

Publisher's Note